BOREAL ENVIRONMENT RESEARCH 27: 145–160
ISSN 1797-2469 (online)

Helsinki 28 September 2022

The role of stratosphere-troposphere coupling in the occurrence of wintertime extreme temperature events over the eastern part of the Baltic Sea region

Indrė Gečaitė

Institute of Geosciences, Vilnius University, M. K. Čiurlionio g. 21/27, Vilnius LT-03101, Lithuania (corresponding author's e-mail: gecaite.indre@gmail.com)

Received 31 Aug. 2022, final version received 6 Sep. 2022, accepted 6 Sep. 2022

Gečaitė I. 2022: The role of stratosphere-troposphere coupling in the occurrence of wintertime extreme temperature events over the eastern part of the Baltic Sea region. *Boreal Env. Res.* 27: 145–160.

Extreme temperature events over the eastern part of the Baltic Sea region during winter were examined in order to address how often these events may be related to the anomalies of stratospheric dynamics through their influence on the tropospheric circulation regime. The propagation of geopotential height anomalies between the stratosphere and the troposphere was evaluated using the Northern Annular Mode. It was determined that in over 60% of all analysed cases, the surface temperature anomalies are preceded by dynamical disturbances in the stratosphere. A strong relation between tropospheric winter temperature extremes and strength of the stratospheric polar vortex was detected up to 10 hPa. Finally, the stratospheric-tropospheric dynamic interaction was evaluated using analysis of Eliassen-Palm vertical wave activity fluxes at a 10 hPa pressure level. The role of the quasi-biennial oscillation phase in the formation of temperature anomalies was also estimated.

Introduction

Surface air temperature anomalies have a significant impact on human life; especially, economic, energy consumption, infrastructure, agriculture, and other spheres, as well as on ecosystems (McMichael *et al.* 2007, Jahn 2015). The long-term forecast of anomalous weather conditions is one of the most challenging tasks of modern meteorology. With the increase of computer processing power in recent years, a lot of attention has been paid to the study of troposphere-stratosphere-troposphere relationships as a possible mechanism that can be used to improve predictions of weather anomalies near the surface with a significant lead time.

It is known that blocking processes in the atmosphere play a decisive role in the formation of anomalous weather conditions. However, despite the rapid development of numerical modelling methods, the long-term prediction of such processes is not always successful (Jia *et al.* 2014, Quandt *et al.* 2017, Kautz *et al.* 2022). Large scale temperature anomalies during the winter season in Europe are well described by low-frequency fluctuations in atmospheric circulation such as the North Atlantic Oscillation (NAO) or Arctic Oscillation (AO). Previous studies have shown that the fluctuations of these indices have a close relationship with processes in the stratosphere (Domeisen *et al.* 2018), namely the strength of the polar vortex (PV) and its geographical location in the North-

Editor in charge of this article: Veli-Matti Kerminen

ern Hemisphere (NH) (Mitchell *et al.* 2013, Butler *et al.* 2015). An anomalously weak PV state, often accompanied by sudden stratospheric warming (SSW), can be associated with large-scale cold spells at mid-latitudes (Baldwin and Dunkerton 2001, Zhang et. al. 2022). The evaluation of the AO sign sensitivity to processes in the stratosphere enable the time frames of index predictability to be extended, as well as improving predictions of temperature anomalies (Thompson and Wallace 2001, Baldwin *et al.* 2003, Douville 2009, Kolstad *et al.* 2010, Mitchell *et al.* 2013, Sigmond *et al.* 2013, Tripathi *et al.* 2014, Kidston *et al.* 2015, Kretschmer *et al.* 2018).

As early as the end of the 20th century, Baldwin and Dunkerton (1999) determined that PV anomalies may penetrate downward from the stratosphere to the troposphere, and this propagation of the anomalies can be evaluated using the Northern Annual Mode (NAM). The NAM is the first empirical orthogonal function (EOF) of the geopotential height (GPH) anomalies at any pressure level. At the surface level, this parameter is the same as AO. During a weak PV, the NAM index is negative, while a positive NAM index indicates periods with a strong PV (Limpasuvan *et al.* 2004). The dynamical coupling between the stratosphere and the troposphere using the NAM index is based on the gradual downward propagation of GPH and zonal wind anomalies (Cai and Ren 2007, Spaeth and Birner 2021). The strength of the PV, in turn, is modulated by thermodynamic processes in the troposphere. This effect is commonly described as Rossby wave vertical propagation and is expressed through the Plumb and Eliassen-Palm vertical wave activity fluxes (WAFs).

Some researchers (Kodera *et al.* 2016, Kretschmer *et al.* 2018, Messori *et al.* 2022) have revealed that the nature and severity of the surface weather anomalies may also be dependent on the type of stratospheric thermodynamical disturbances, such as whether the vertical WAFs are absorbed or reflected back to the troposphere. Not only the intensity of the reflection of the downward WAFs, but also their geographical location (Shi *et al.* 2017) can play a significant role in the formation of NH weather anomalies.

Absorbing-type disturbances (Kodera *et al.* 2016) are related to prolonged upward WAF "attacks", and as a result, increased polar cap temperatures and a weakened PV in the stratosphere. Later on, the zonal-mean flow anomalies, mathematically correspond to the negative NAM phase, propagate downward into the troposphere, and can persist there for 60 days (Baldwin and Dunkerton 1999, Baldwin and Dunkerton 2001, Ambaum and Hoskins 2002, Perlwitz and Harnik 2004, Shaw and Perlwitz 2013, Karpechko *et al.* 2017). According to the studies of Baldwin and Dunkerton (2001), Gerbert and Polvani (2009) and Kim and Choi (2021), the anomalies associated with a weak PV can propagate downward into the troposphere, influencing the sign of the NAM/AO, storm track shifts, and herewith regional temperature anomalies, especially over northern Eurasia. It was also found by Ambaum and Hoskins (2002) that a strong positive NAO index, on the contrary, leads to a more intensive stratospheric PV with a lag of about four days. However, a strong PV can reflect the upward-propagating WAFs downward and affect the circulation regime at the surface (Perlwitz and Harnik 2003, Kodera and Mukougawa 2008, Harnik 2009, Kodera *et al.* 2013).

Reflective-type disturbances (Kodera *et al.* 2016) are associated with shorter but more intense upward WAFs from the troposphere to the stratosphere, a faster recovery of the PV, and the reflection of the WAF back to the troposphere. Some studies (Kodera *et al.* 2008, Kodera *et al.* 2013) have found that the reflective-type phenomena are associated with a negative phase of Pacific Oscillation (western-WPO and northern-NPO). Nath *et al.* (2016) showed that reflected downward WAFs during the 2013 winter led to the formation of a deep trough over Eurasia and brought extreme cold weather over some parts of Asia. However, a broader impact assessment should be carried out to provide more clarity on the impact of the reflecting-type stratospheric thermodynamical disturbances on the weather regime of different NH regions.

Moreover, some studies have confirmed the response of the winter AO phase and the European winter surface weather to stratospheric quasi-biennial oscillation (QBO) (Marshall and

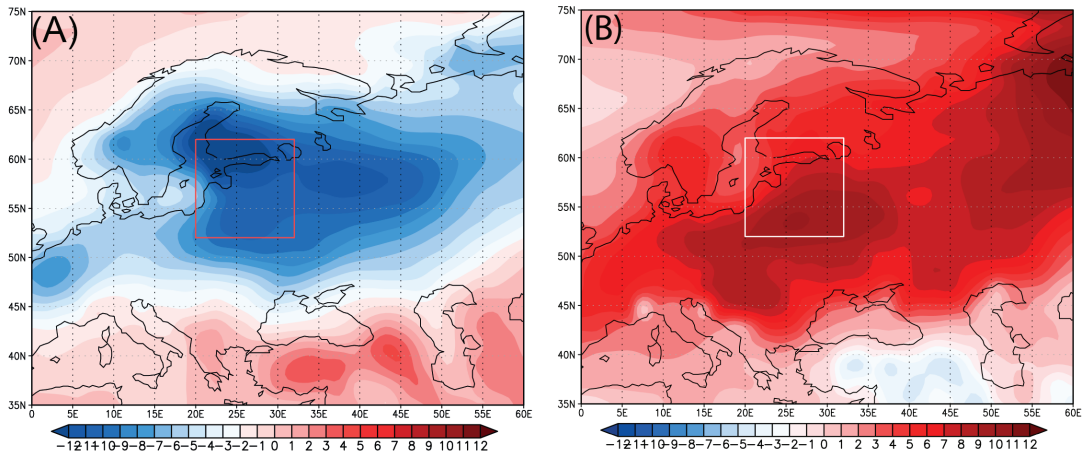

Fig. 1. Surface air temperature anomalies (°C) during CS in (**a**) January 1987 and (**b**) WS in January 2007 in Europe; red/white boxes delineate the study area.

Scaife 2009). When the QBO is in its easterly phase in the lower stratosphere, it favours stronger Madden-Julian Oscillation (MJO) activity during boreal winters, which tends to be weaker during the westerly phase of the QBO (Klotzbach *et al.* 2019). An earlier study by Cassou (2008) revealed that MJO controls part of the distribution of weather regimes over the North Atlantic–European region in winter, which can be expressed through the NAO index. A recent study by Barnes *et al.* (2019) confirmed that MJO can impact the NAO via both a tropospheric and stratospheric pathway.

Despite the complex feedback relationships between the troposphere and the stratosphere, the processes in the stratosphere are much more predictable than at the surface level. By identifying the nature of the relationships and the time intervals between the different processes operating between these two atmospheric layers, we could significantly improve the long-term forecast of extreme weather events (Scaife *et al.* 2022). A lot of research is being conducted in this field, however, the full potential of stratospheric information for improving the prediction of extreme temperature events has not yet been reached. Here, we present analysis of NAM index fluctuations (of tropospheric and stratospheric origin) linked to the CSs and WSs in the eastern part of the Baltic Sea region over 1951–2020. Moreover, GPH anomalies over the NH before CSs and WSs on different pressure levels were determined. The stratosphere-troposphere relationships based on the intensity and location of vertical Eliassen-Palm WAFs were also evaluated. In addition, the importance of the QBO phase (as a remote connection) for the formation of temperature extremes was evaluated.

Data and methodology

Data and study area

In the first part of this study, we determined the CSs and WSs in the eastern part of the Baltic Sea region. This region lies between 52° and 62°N and between 20° and 32°E (red/white boxes in Fig. 1). We used E-OBS daily minimum (Tn) and maximum (Tx) temperature gridded data from the latest E-OBS (ver. 23.1e) dataset on a 0.25°–0.25° longitude–latitude grid (Cornes *et al.* 2018). The NAM index was computed using the daily National Centres for Environmental Prediction (NCEP)/National Centres for Atmospheric Research (NCAR) reanalysis data. The WAFs were calculated using the Modern-Era Retrospective Analysis for Research and Applications version 2 (MERRA-2) three-hourly reanalysis data. This is one of the most recent reanalysis products with an improved representation of stratospheric dynamics. MERRA-2 contains 72 vertical layers up to 0.01 hPa and has a 0.5° × 0.625° horizontal resolution (Gelaro

et al. 2017). The stratospheric zonal wind speed at 60°N (near the peak of the polar jet) was also evaluated using MERRA-2 data. These data were obtained from the National Aeronautics and Space Administration (NASA) Goddard Space Flight Centre. The QBO phase data were used from the Freie Universitat Berlin data base.

This region was chosen for practical reasons to detect potential predictors for extreme temperature forecasting. Previous studies (Tomassini *et al.* 2012) have shown that there is a significant relationship between the cold spells and circulation anomalies in the stratosphere up to at least 50 hPa in northern Europe. According to their results, 42% of all analysed CSs were associated with a downward propagating dynamical disturbance which originated in the stratosphere.

In addition, Kretschmer *et al.* (2018) found that a weak stratospheric PV doubled the chances of a CS in northern Eurasia. Based on the presented temperature anomaly maps (Kretschmer *et al.* 2018: fig. 5b), this region experiences some of the lowest temperatures during weak PV conditions. The association of cold extremes with the stratosphere has been related to negative NAO phases and high latitude blocking. Nevertheless, extreme temperature anomalies are usually not limited to this area and cover most of Europe or northern Eurasia (Fig. 1).

Methods

We analysed wintertime extreme temperatures, which is defined as the December-February (DJF) season. The CSs/WSs were determined whenever Tn (Tx) was above the 90th percentile (below the 10th percentile) for at least five consecutive days and with a time lag of no more than two days between two separate events. The daily percentile values using 1971–2000 baseline on a five-day centred window were computed. Thus, we detected all WSs and CSs in every grid point throughout the period 1951–2020. In this research, we used only those events (35 CSs and 30 WSs) which were observed in over 70% of all analysed area (see Supplementary Information Fig. S1).

In the second part of the research, we calculated the NAM index at different pressure levels (n = 15) starting from 850 hPa up to 10 hPa. Mathematically, the NAM index fully corresponds to the AO index, because they are both the first EOFs of the hemispheric pressure/geopotential height field. The NAM index is expressed as the first EOF of NH daily GPH anomalies from 20° to 90 °N. Since the grid size decreases as you move towards the pole, the data were weighted by the square root of the cosine of latitude (for more information see Baldwin *et al.* 2009). The daily seasonal cycle climatology computed for the 1951–2020 period was removed from each grid point. A linear trend was subtracted for every grid point from each dataset. An eigenvalue decomposition analysis was used to obtain the EOF spatial patterns and first principal component (PC1) of time series. We analysed the variation of the NAM index across the entire atmospheric layer from 10–850 hPa before and after a WS/CS. We chose a time span of 50 days before the event and 20 days after. We chose this time interval, because as previously determined, the NAM phase propagates downward from the stratosphere into the troposphere and can persist there for up to two months (Baldwin and Dunkerton 2001). Composites of GPH for Z10, Z150, Z300, and Z500 were made using NCEP/NCAR reanalysis 1 daily GPH data. The anomalies were obtained using a 1981–2010 baseline.

In the third part, we used extreme values of upward and downward Eliassen-Palm WAF at 10 hPa. The WAF calculation methodology was described in detail in our previous article (Gecaite 2021). We compared the average of daily maximum upward WAFs 30 days before a CS/WS with the average of daily minimum downward WAFs 15 days before and 20 days after a CS/WS (during the period from 1980–2020). In addition, we evaluated the QBO phase at a 10 hPa pressure level during the start date of the CSs and WSs.

The evaluation of the vertical structure of the NAM index fluctuations

Correlation analysis was used to evaluate the vertical structure of the NAM index fluctuations and its relationships between different pressure

levels (see Supplementary Information Fig. S2). This gives us more information about extent to which the circulation of the stratosphere and troposphere may be related to each other.

The values of the NAM index (see Supplementary Information Fig. S2) have a very close relationship between the nearest pressure levels (r = 0.95–0.99, p < 0. 00001), which indicates that the anomalies of GPH are transmitted between neighbouring levels. It was determined that the NAM values at levels of 200 hPa and 150 hPa (near the tropopause) have the highest correlation (r = 0.43–0.97, p < 0. 00001) with other pressure levels. Therefore, this level can be considered a transitional level, where the NAM anomalies of both stratospheric and tropospheric origins can be observed.

We also performed cross correlation analysis between NAM indices at 850 hPa and 10 hPa pressure levels for every cold season (November-March) during 1951–2020. Our results show that more often than not (61% of all analysed cold seasons), the highest correlation coefficients were reached with the NAM_{850hPa} time series shifting backward relative to the NAM_{10hPa} series. This means that the GPH anomalies propagated down from the stratosphere to the troposphere. The strongest positive relation was found with an average delay of 21 days. Since the NAM is calculated from GPH anomalies, this is partly an expression of temperature anomalies in underlying atmospheric layers. The NAM index is often used to determine the strength of stratosphere-troposphere coupling, and can be useful for evaluating the vertical propagation of GPH anomalies during periods of extreme weather events.

Results

NAM index and GPH anomalies during cold spells

The analysis of the NAM index time series during all CS events revealed that not all CSs were associated with a negative NAM index in the entire vertical column (from 850 hPa up to 10 hPa) as may be expected. This allowed us to classify all CS events into two groups. The first group (stratospheric CSs) included those CSs before which negative a NAM phase had the potential to propagate down from the stratosphere to the troposphere. The second group (tropospheric CSs) included CSs, the formation of which was unlikely to be associated with a negative NAM index in the stratosphere.

We found that 66% of all CSs may be associated with a negative NAM phase. The averaged NAM index was negative during the whole time period (50 days before and 20 days after the CS). The first minimum point at 10 hPa was recorded on average 29 days before the CS and the second, which was more intense, a few days before the CS (Fig. 2). The fluctuations of the NAM index between these minimum points were also very synchronous in an atmospheric layer from 850 hPa up to 20 hPa. Thus, it is likely that weak PV conditions (indicated by a negative NAM phase) in the stratosphere before the CS may have influenced the near-surface weather regime. An analysis of correlation, together with a cross-correlation approach, showed that the relationship between the NAM time series of the 850 and 10 hPa pressure levels (averaged over all CSs) was positive (r = 0.21; p = 0.081). The correlation reached its maximum value with a delay of nine days (NAM_{10hPa} phase propagated down to 850 hPa) and was equal to 0.50 (p < 0.0001).

A weak PV was observed together with positive symmetric 10 hPa level GPH anomalies above the North Pole (anomalies on average reached up to nearly 500 m). A weak PV, which is often associated with cold anomalies at mid-latitudes in the NH, was common for the entire 30-day period before the onset of the CS (Fig. 3). Negative average zonal wind speed anomalies at 60°N were also found. The zonal wind speed was slower by 4 m/s on average 30 days before the CS and slower by 11 m/s 15 days before the CS. The PV was found to remain weaker than its long-term normal (1979–2020) during the cold wave (15-day mean from the date of the CS onset) with an anomaly of –10 m/s.

The analysis of NH GPH (Z500, Z300, and Z150) composites (see Supplementary Infor-

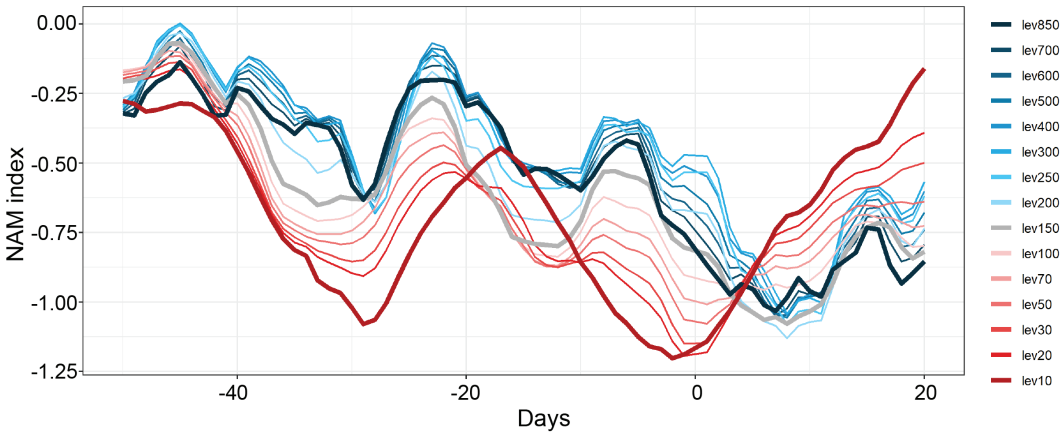

Fig. 2. NAM index fluctuations during time periods with a stratospheric related CSs (50 days before and 20 days after the onset date of the CS indicated as day 0) between 850 hPa and 10 hPa pressure levels (NH); the solid thick navy blue line marks the variation of the NAM index at a 850 hPa pressure level (other levels in the troposphere are marked by thinner lines with blue colour shades), the solid thick grey line indicates the NAM variation at a 150 hPa level (near the tropopause), and the solid red line indicates variations of the NAM index in the stratosphere 10 hPa (other levels in the stratosphere are marked by thinner lines with red colour shades).

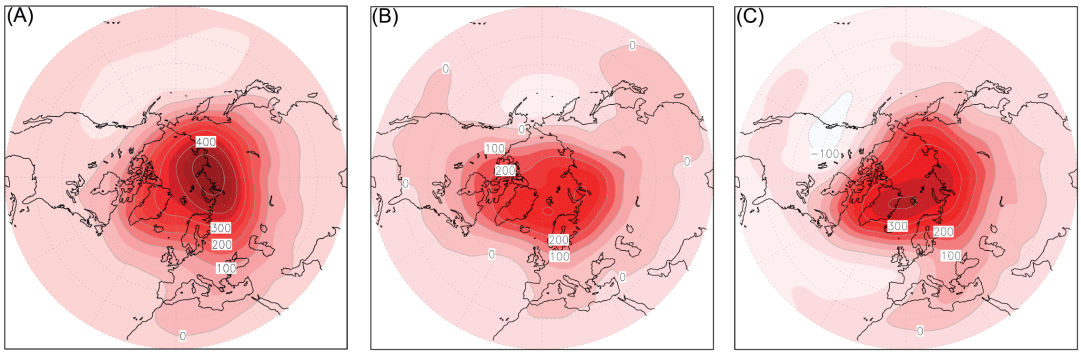

Fig. 3. Average GPH anomalies (m) at a 10 hPa pressure level (**a**) 30 days before the CS; (**b**) 20 days before the CS; and (**c**) 10 days before the CS in the NH (20–90°N).

mation Fig. S3) showed that positive height anomalies were observed over the Barents-Kara Seas (BKS) 20 and 30 days before the CS, and over Greenland ten days before the CS. These anomalies are best seen at the 300 and 150 hPa levels. However, 34% of all CS cases (Fig. 4) were not associated with a negative NAM index descending from the stratosphere, as the stratospheric negative NAM index was usually either not recorded for almost all of the 50 days before the CS or the negative index first appeared in the troposphere and then gradually propagated to the stratosphere. The mean values of the index have a much wider variation range with height, although the synchronicity itself is still quite clear. Cross-correlation analysis revealed that the strongest relationship between NAM_{10hPa} and NAM_{850hPa} time series was from the bottom to the top, with a 16-day time delay ($r = 0.41$, $p = 0.002$).

Prior to the CSs of this group, a strong PV was seen at the 10 hPa level, and positive GPH anomalies were recorded over Europe 10 and 30 days before the CS (Fig. 5). According to the strong PV state, together with the negative

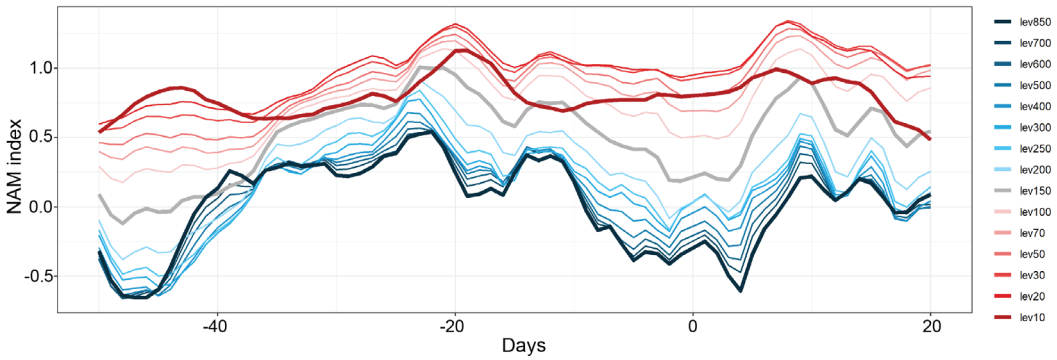

Fig. 4. NAM index fluctuation during the time period with a non-stratosphere-related CSs (50 days before and 20 days after the onset of the CS indicated as day 0) between the 850 and 10 hPa pressure levels (NH); the solid blue line marks the variation of the NAM index at a 850 hPa pressure level (the lower troposphere), the solid grey lines indicate NAM variations in the troposphere (700–150 hPa), and the solid red lines indicate the variations of the NAM index in the stratosphere (100–10 hPa).

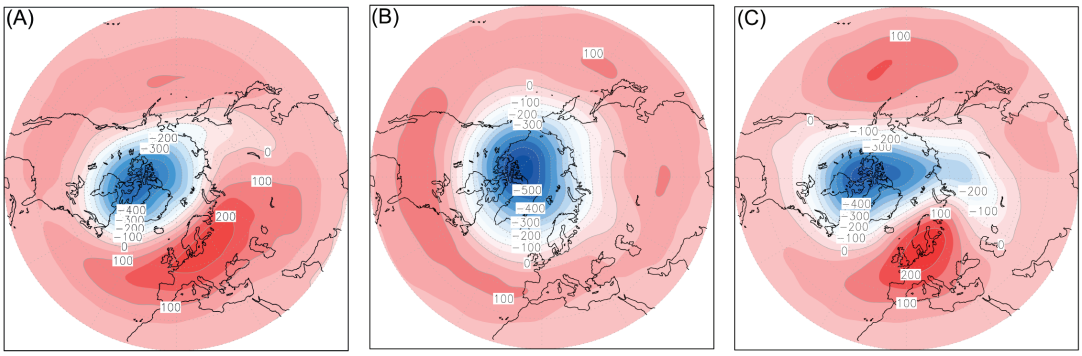

Fig. 5. Average GPH anomalies (m) during non-stratospheric CSs at 10 hPa pressure level (**a**) 30 days before CS; (**b**) 20 days before CS; and (**c**) 10 days before CS in the NH (20-90°N).

anomalies of GPH lowering to 500 m, it is very unlikely that the PV had a tendency to weaken or break down. Analysis of the anomalies of the average zonal wind speed at 60°N showed that the weakening of the polar jet stream was insignificant. During the 30-day period preceding the CS, the average anomaly was only –0.4 m/s, and for the 15 days before the CS, the anomaly was –3.6 m/s. During the CS, the intensity of the PV became close to normal.

During the non-stratosphere related CS events, negative Z500, Z300, and Z150 anomalies were observed over the BKS and the North Atlantic, and positive anomalies were recorded over Europe and the North Pacific (see Supplementary Information Fig. S4). Ketchmer *et al.* (2018) revealed that increased GPHs over the North Pacific are characteristic of reflecting-type events in the stratosphere. According to Kodera *et al.* (2015), reflecting-type SSWs are characterised by a short stratospheric warming episode and quick recovery of the PV due to the reflection of WAFs, which leads to an amplification of tropospheric planetary waves and blocking over the North Pacific sector. This may trigger the eastward propagation of stationary Rossby waves from the North Pacific into the North Atlantic.

Marshall *et al.* (2009) proposed that negative DJF temperature anomalies in northern Europe are more likely to occur during the eastern QBO (EQBO) phase. We verified this finding with our CS data and found that 78% of all CSs in the eastern Baltic Sea region occurred during the EQBO phase (at 10 hPa), confirming this statement.

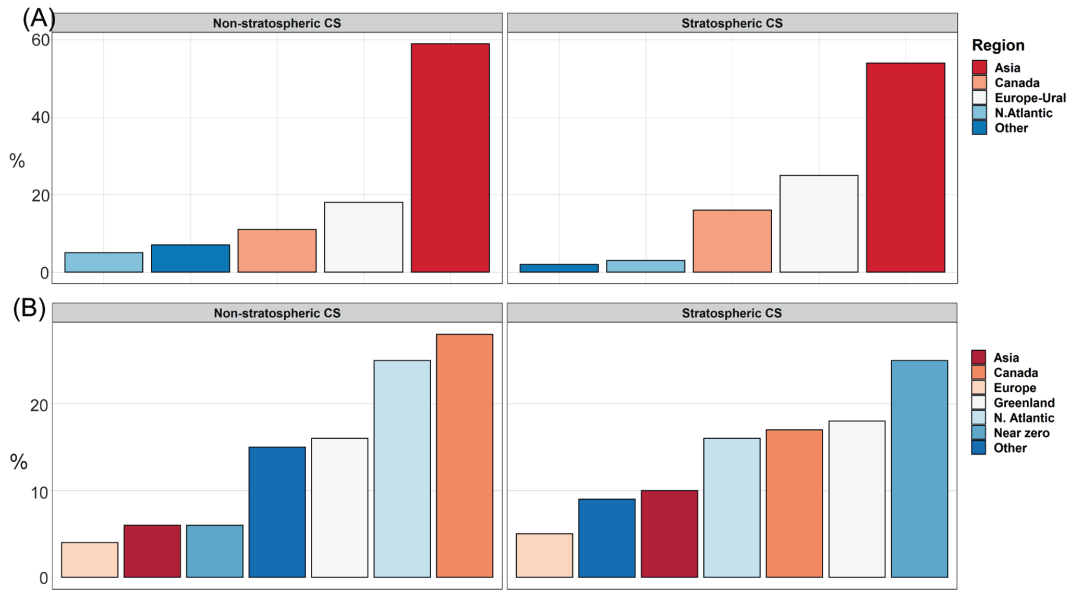

Fig. 6. Spatial distribution of extreme (**a**) upward and (**b**) downward Eliassen-Palm WAFs 30 days before non-stratospheric and stratospheric CSs during the 1981–2020 period.

The strength and spatial distribution of the WAFs during CSs

The analysis of the spatial distribution of anomalous strong upward WAFs during CSs revealed that in the group with a possible impact from the stratosphere, the upward WAFs were most intense over Asia and the Europe-Ural region, while in the other group they were exceptionally strong over Asia (Fig. 6a). The latter corresponds well to climatological values, according which (Gecaite, 2021), 59% of all high-intensity upward WAFs over the NH are recorded over Asia.

A significant difference was found when comparing the distribution of downward WAFs in both CS groups. It was found that in the group with a stratospheric influence, the so-called "near-zero" downward WAF condition (25% of all cases) was recorded four times more often than in the other CS group. The "near-zero"state is considered when there is no downward propagation observed and this may be a feature of the absorbing stratospheric PV state. In the non-stratospheric CS group, the maximum was recorded over Canada and the North Atlantic (Fig. 6b).

We also analysed the strength of maximum upward and minimum downward WAFs 30 days before and 20 days after the CS. The average long-term (1981–2020) WAF values for November–February were 2.5 m^2s^{-2} for upward and –0.95 m^2s^{-2} for downward propagating WAFs. It was determined that the group of CSs that could potentially be affected by stratospheric anomalies had stronger upward and downward WAFs in comparison to the values of another CS group (Fig. 7). A 30-day average upward WAF intensity was stronger by 24% and an average absolute maximum upward WAF value was 2.4 times more intense than the climatological mean values for cold seasons. Meanwhile, during the 20-day period after the start date of the CS, a more intense (60% more than climatological data) upward WAF was observed in the group which had a weaker interaction with the stratosphere. This means that the effects on the stratosphere from the troposphere intensified only during the period of the CS.

Comparing the strength of the most intense downward WAFs, it was found that on average, they were stronger in the group without a stratospheric influence (by 47%); however, the averaged absolute minimum over the 30-day

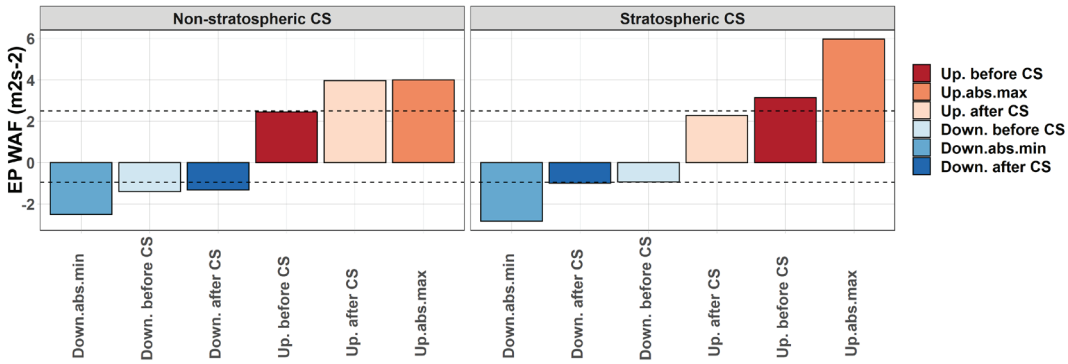

Fig. 7. Intensity of upward and downward Eliassen-Palm WAFs (averaged 30 days before the CS, the averaged absolute maxima and minima, and the WAF intensities averaged 20 days after the start of the CS) during the 1981–2020 period. The dashed horizontal lines accordingly show the long-term (1981–2020) mean values of November–February maxima upward and minima downward WAFs.

period before the CS was higher in the group with a possible stratospheric impact and was three times stronger than the climatological mean (Fig. 7). During the onset of the CS and 20 days after, the more intense downward WAFs occurred for non-stratospheric CSs. The average downward WAFs were also 37% stronger than the climatological mean.

NAM and GPH anomalies during warm spells

Cold and warm spells are both extreme temperature events, albeit of the opposite sign. Theoretically, CSs are more likely to occur when the PV is weakened, and warmer weather conditions are more readily associated with a strong PV state. However, CSs and WSs are both products of meridional circulation, so a strong PV will not necessarily lead to WSs. To test this hypothesis, we analysed variations of the NAM index 50 days before and 20 days after the WSs. We also investigated the compositions of GPH anomalies at different pressure levels as was done in the previous section.

In the case of WSs, a positive NAM index is usually dominant in the stratosphere indicating a PV which is stronger than normal. However, three different groups of stratospheric NAM index fluctuations can be distinguished. During 47% of all cases (Group I), the NAM index became positive (in the stratosphere and in the troposphere) on average one month before the WS and remained positive all throughout the 20 days after the WS. Another 33% (Group II) of all cases had the opposite tendency, with the NAM index at the 10 hPa level being positive on average 20–50 days before the WS and then negative three weeks before and during the WS. Meanwhile, the variation of the NAM index in the troposphere had the opposite sign. In the troposphere, the NAM index became positive approximately two weeks before the WS. Only in 20% of all analysed WS cases (Group III), highly positive stratospheric NAM indices were observed around all 50 days before the WS and 20 days following it (Fig. 8a–c).

Groups I and III are in good agreement with the theory and may be related to the state of a strong PV, i.e., its recovery (Group I) or its persistent high intensity (Group III). Correlation analysis between the NAM index time series at 850 hPa and 10 hPa pressure levels showed that the highest correlation coefficient ($r = 0.92$, $p < 0.00001$) was achieved with a ten-day time lag in group I and only over a two-day time span in Group III ($r = 0.61$, $p < 0.00001$). Meanwhile, the correlation coefficients in Group II were negative, suggesting that the GPH anomalies were asynchronous between the stratosphere and the troposphere over a short time interval, the correlation coefficient became significantly positive only with a 30-day delay. These relationships are well captured in a composite of 10 hPa GPH anomalies recorded during different periods before the WS (Fig. 9). Analysis of

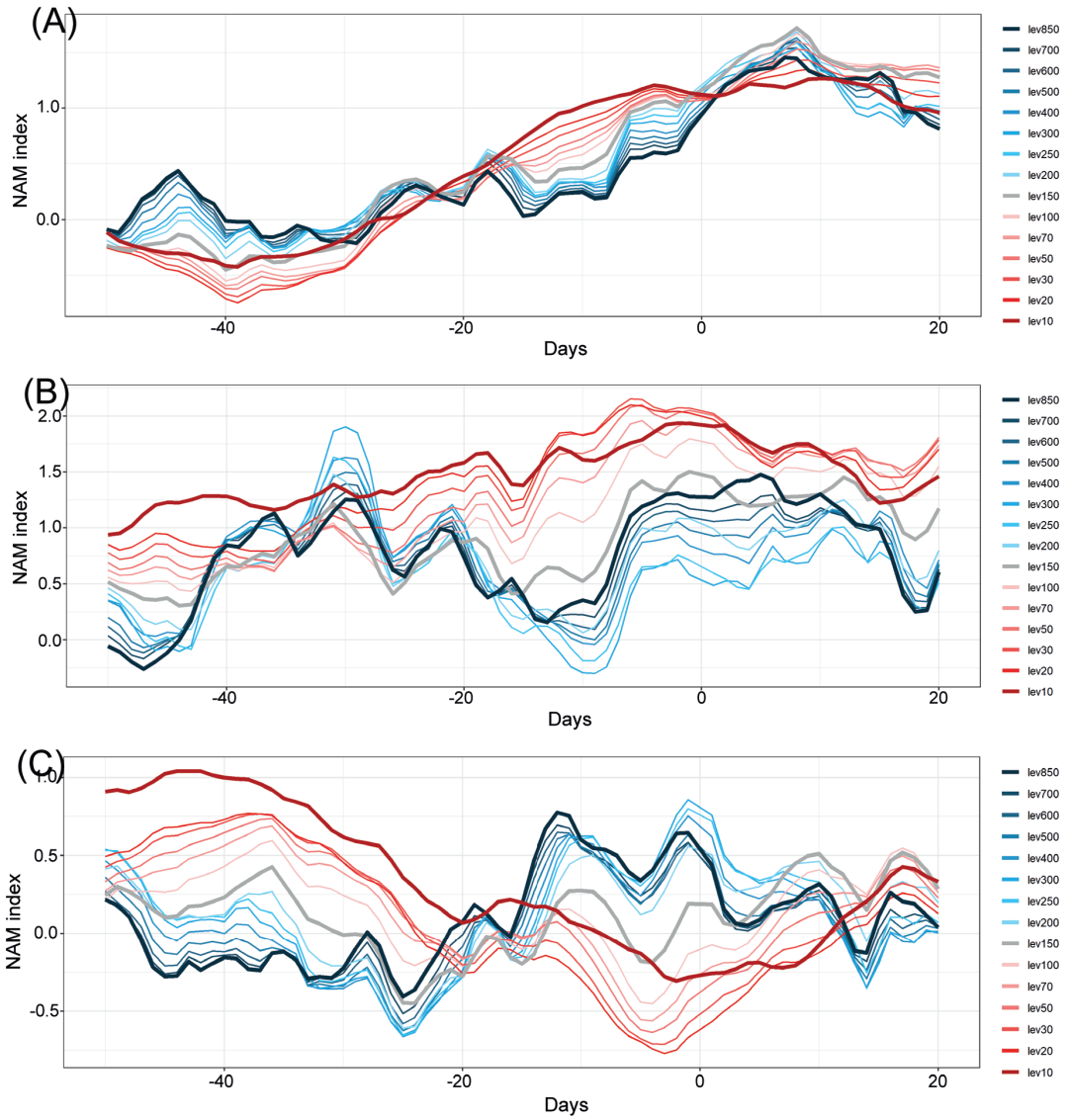

Fig. 8. NAM index fluctuations during time periods with (**a**) Group I WSs; (**b**) Group II WSs; (**c**) Group III WSs (50 days before and 20 days after the onset of the WS indicated as day 0) between the 850 and 10 hPa pressure levels (NH); the solid blue line marks the variation of the NAM index at the 850 hPa pressure level (lower troposphere), the solid grey lines indicate NAM variations in the troposphere (700–150 hPa), and the solid red lines indicate variations of the NAM index in the stratosphere (100–10 hPa).

these anomalies in Group I revealed that the PV began to intensify approximately 20 days before the WS. In the ten days before the WS, the mean Z10 anomaly reached > 500 m, indicating a strong PV (Fig. 9a–c). The zonal wind anomaly 30 days before the WS was also positive. Meanwhile, Group II showed signs of PV breakdown with asymmetric anomalies: a strongly positive Z10 anomaly was recorded over the pole and two cores of the negative anomaly over the North Atlantic and Asia (Fig. 9d–f). The averaged zonal wind speed showed that the polar jet stream was slower than normal by 4.4 m/s. The strongest vortex was found in Group III for the entire 30-day period before the WS. The Z10 anomalies were localised over Canada with

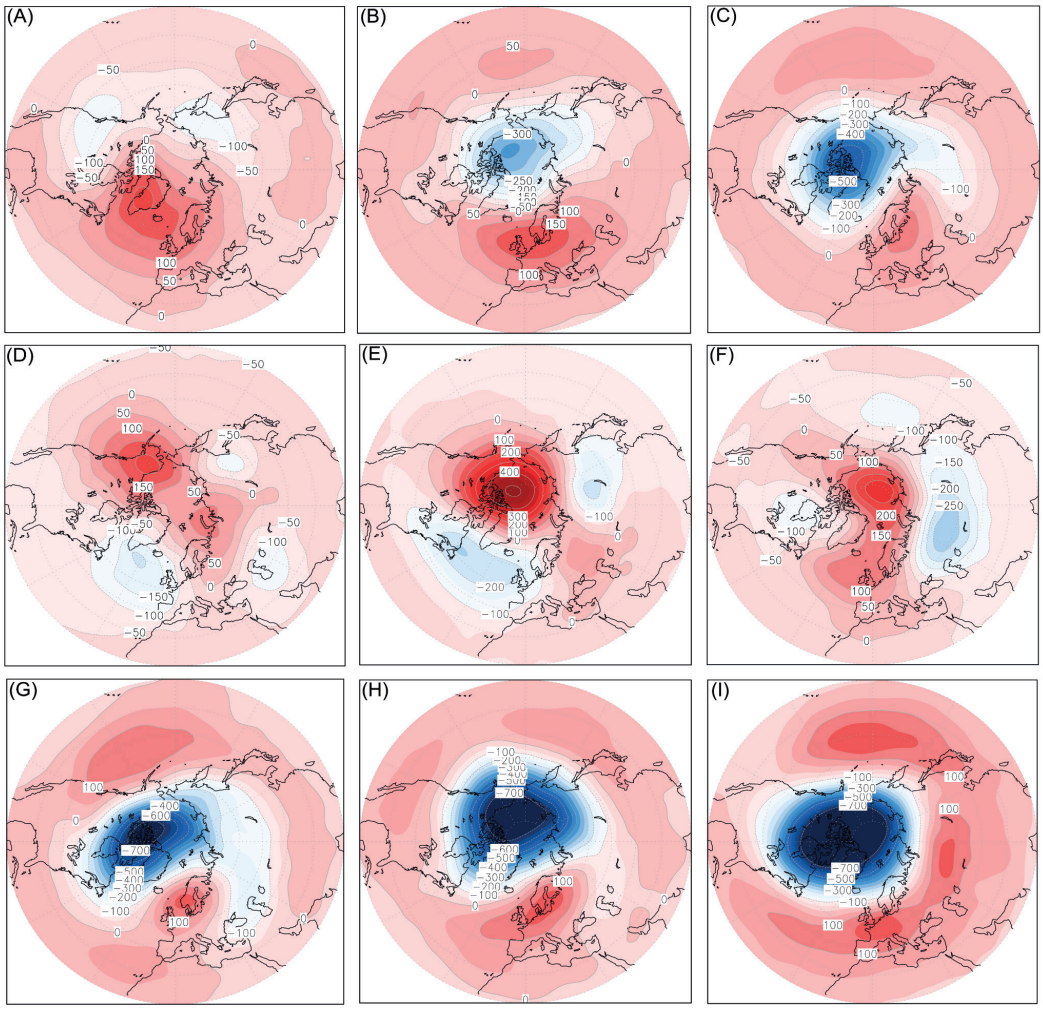

Fig. 9. Average GPH anomalies (m) during different Groups of WSs at the 10 hPa pressure level; Group I: (**a**) 30 days, (**b**) 20 days, and (**c**) 10 days before the WS; Group II: (**d**) 30 days, (**e**) 20 days, and (**f**) 10 days before the WS; Group III: (**g**) 30 days, (**h**) 20 days, and (**i**) 10 days before the WS, in the NH (20-90°N).

a magnitude of more than 700 m (Fig. 9g–i). Zonal wind anomalies at 60°N also showed a very intense polar jet stream with an anomaly of 15.5 m/s (averaged over 30 days before the WS).

Analysis of GPH anomalies at different pressure levels (Z500, Z300, and Z150) revealed that anomalies were observed simultaneously at all three levels. In Group I, 30 days prior to the WS, positive GPH anomalies were observed over the North Atlantic and tended to move eastward reaching northern Europe 20 days before the WS. GPH anomalies over northern Europe persisted almost until the beginning of the WS. At the same time (around 20 days before the WS), negative GPH anomalies prevailed in the North Atlantic, gradually moving eastward, pushing the field of positive anomalies further south, and thus creating favourable conditions for the intensive western transport of warm air masses. Such a system resembles the state of a positive NAO (NAO+).

Despite PV differences in the stratosphere, the spatial distribution of GPH anomalies 30 days before the WS in Group II was quite similar to that of Group I, but with a shorter NAO+ preconditioning. During the development of favourable circulation conditions for WSs in Group II, two predominant cores of positive

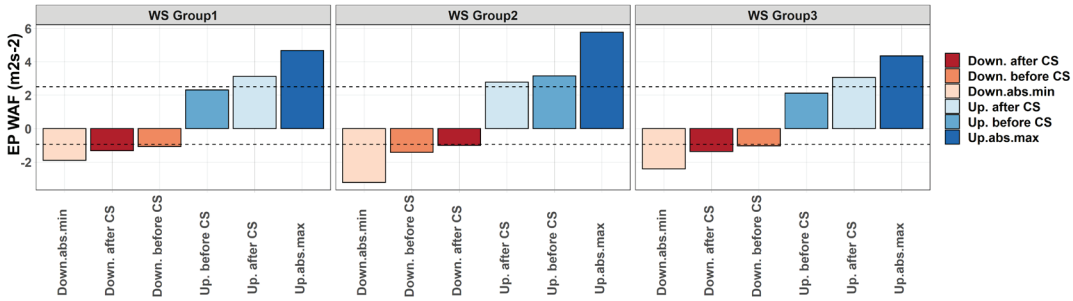

Fig. 10. Intensity of upward and downward Eliassen-Palm WAFs (averaged 30 days before the WS, the averaged absolute maxima and minima, and WAF intensity averaged 20 days after the start of the WS) during the 1981–2020 period. The dashed horizontal lines accordingly show the long-term (1981–2020) mean values of November–February maxima upward and minima downward WAFs.

GPH anomalies were observed: one in the North Atlantic-European sector and the other over the Pacific Ocean. The seesaw of these two centres of anomalies were observed not only in the Z10 but also in the troposphere.

Significant differences were found for the WSs of Group III. Positive GPH anomalies at all three pressure levels persisted over Europe for 20–30 days prior to the WS. Meanwhile, a significant decrease in GPH up to 250 m was observed ten days before the WS over northern Europe. A few days before the WS, positive GPH anomalies began to form over southern Europe. This configuration caused an extremely intense advection of warm air masses from the western sector. Atmospheric circulation was also observed to be somewhat more dynamic, with several cores of positive GPH anomalies over the North Atlantic, the Asian continent, and the Pacific Ocean.

We also checked the QBO phase during the months with the WS and determined that WSs were recorded almost equally during both the western (52%) and eastern (48%) phases.

The strength and spatial distribution of the WAFs during warm spells

The highest intensity of both upward and downward WAFs was found in Group II (Fig. 10). The intensity of upward WAFs was similar to that observed before stratosphere-related CSs, while downward WAFs were the strongest among all classified groups of CS and WS analysed in this study. These results are also in good agreement with the identified anomalies of GPH and zonal winds before the onset of WSs. The weakest upward WAFs (16% less than the long-term norm of the cold season) were recorded in Group III. The lack of WAF intensity may have led to a strong PV, and also suggests that there were no high amplitude Rossby waves in the troposphere, hinting at the prevalence of the zonal transport of the air masses. Although the weakest downward WAFs were observed in Groups III and I, wave activity was only 8% and 13% more intense than the climatological mean in these groups, respectively.

In the first WS group, the strongest upward WAFs were recorded over Asia, while the strongest downward WAFs were recorded over the North Atlantic and Greenland (Fig. 11a). In the second WS group, the most intense WAFs were also observed over Asia, coinciding with climatological values; however, high intensity WAFs were also observed over the Europe-Ural sector (24%). Downward WAFs (Fig. 11b) were most prominent over Canada, but an unusually large number of intense downward WAFs were recorded over Europe in this group. In the third WS group, the peak of upward WAFs fell over Asia, but it was also observed that in this group, intensive upward WAFs appeared much more frequently over the Pacific and Canada than in other groups. The geographical locations of WAF extremes in Group III were much more evenly distributed over the NH. The strongest downward WAFs were found over the North Atlantic and Greenland.

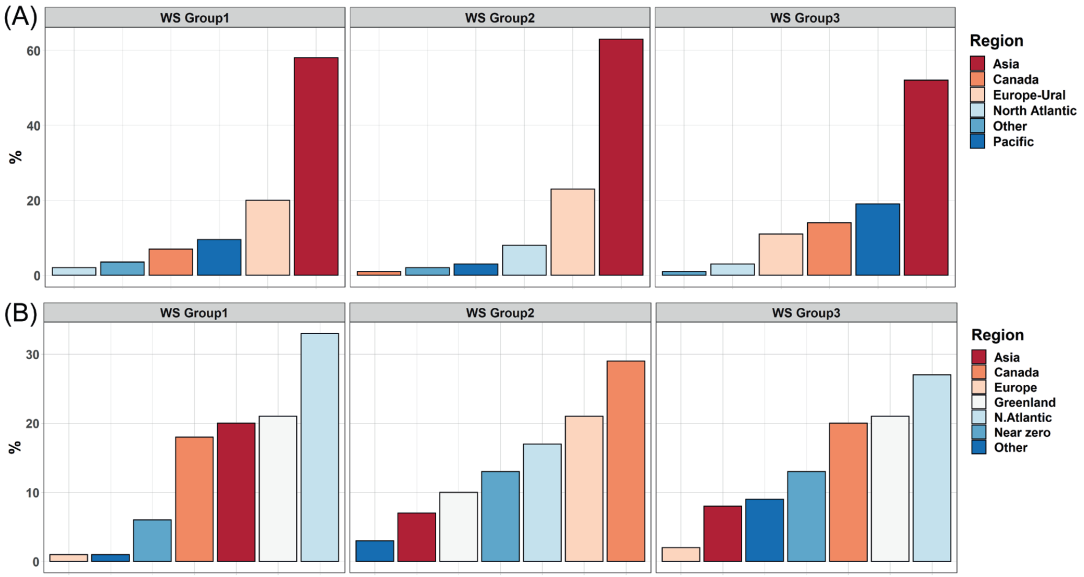

Fig. 11. Spatial distribution of extreme (**a**) upward and (**b**) downward Eliassen-Palm WAFs (30 days before the WS) during the 1981–2020 period.

Conclusions and discussion

In this paper, NCEP/NCAR and MERRA-2 daily reanalysis data was used to analyse the evolution of the stratospheric circulation anomalies and the likelihood of its descent downwards into the troposphere during periods of extreme temperatures in the eastern part of the Baltic Sea region. To evaluate this, we considered the NAM index on 15 pressure levels from 850 hPa to 10 hPa. We also evaluated the GPH Z150, Z300, and Z500 anomalies one month before the CS/WS. Finally, the strength of the polar jet stream, intensity of Eliassen-Palm vertical WAFs, and their geographical distribution over the NH was investigated.

We determined that 66% of all CSs may be associated with a weak PV and negative NAM index descending from the stratosphere to the troposphere. The time that it takes for GPH anomalies to descend from 10 hPa to 850 hPa equals ten days on average. The different indicators used in this study suggest that the PV condition and the processes at the 10 hPa level during these CSs are very similar to the absorbing-type conditions during the weak stratospheric PV described by Kodera (2009) and Krechmar *et al.* (2018). We also determined that upward WAFs were 24% more intense than the climatic norm before the CS (Gecaite 2021), but the downward WAFs were close to the latter. We also found that the so-called "near-zero" WAF condition dominated 15 days before the CS (four times more often than in the other CS cases in this study). This state is associated with intense upward WAFs (Scott and Polvani 2004) and the abrupt attenuation of the PV vortex. Intense WAFs were observed over Central Asia and the Europe-Ural sector.

We found that positive GPH anomalies before the CS with possible stratospheric influence may be related to the enhanced probability of Ural blocking; this may trigger a stationary Rossby wave train that can weaken the stratospheric PV, which is often followed by extreme weather events at mid-latitudes in the NH. The downward influence of the weak PV leads to a weaker westerly flow at the NH mid-latitudes. It is possible that the CSs of this group were related to an increased probability of Greenland blocking, which had a potential to develop ten days before the CS and was associated with the negative phase of the NAO (NAO-) (Luo *et al.* 2007). The increased activity of Greenland blocking and NAO- may also be related to enhanced Ural blocking and a weak PV. This mechanism was described in detail by Tyrlis *et*

al. (2019). For comparison, positive Z500, Z300, and Z150 anomalies were observed over Europe and the North Pacific in the group with CSs of non-stratospheric origin. Positive GPH anomalies ten days before the CS over northern Europe may indicate an increased likelihood of a Scandinavian blocking pattern (SCAND+), which, as previous studies have shown (e.g., Pang *et al.* 2021), does not have a close relationship with the stratosphere.

We found that a strong PV is more closely related with WSs, when a positive NAM index is dominant. Our analysis showed that 67% of all stratospheric conditions were able to provide favourable conditions (as one of the factors) for WS formation. We divided all WSs into three groups according to NAM index sign distribution before and after the event. Group I and III were classified as stratospheric. The delay between NAM phase fluctuations at 10 hPa and 850 hPa levels (from top to bottom) was found to be very small, reaching ten days in Group I and only two days in Group III. Analyses of Z10 anomalies showed that a very strong PV before the WS was observed in Groups I and III and the polar jet stream speed was greater than long term mean 30 days before the WS. A strong stratospheric polar jet is associated with the gradual radiative cooling of the polar cap and for this reason may persist for a long time. This was confirmed by the strength of WAFs 30 days before the WS, which was below the climatic norm. Downward WAFs were close to climatic norm and were most often observed over the North Atlantic.

GPH anomalies were synchronously observed from 500 up to 150 hPa before the WS (Groups I and III). This result is in good agreement with the results obtained in other studies (e.g., Tomyzeck *et al.* 2019, Qian *et al.* 2016, Chen *et al.* 2017) that also found that GPH anomalies were traceable up to the tropopause with a significant time lag. A distribution of GPH anomalies before WSs were reminiscent of a NAO+ state, which is favourable for the inflow of warm air masses from the North Atlantic.

We also determined that 78% of all CSs occurred during the EQBO phase (at 10 hPa). Such a great coincidence may give us a significant basis for predicting cold anomalies. When the QBO was in its easterly phase in the lower stratosphere, it favoured stronger MJO activity during boreal winters (Klotzbach *et al.* 2019). This, in turn, has a close relationship with NAO phases (Lee *et al.* 2019). However, during the months during which the WS started, WQBO and EQBO were recorded almost equally, 52% and 48%, respectively.

Resolving the directionality of causality is not a trivial task because the specific conditions in the troposphere causing stratospheric thermodynamic state anomalies may be responsible for later surface anomalies as well. In our research, we used the term "possible influence" because it is not always very clear whether extreme temperature events were impacted by: i) the stratospheric anomalies, ii) the tropospheric circulation during the onset of stratospheric anomalies, or iii) stratosphere–troposphere feedbacks that lead to the NAM phase descending from the top to the surface. However, our study revealed that certain characteristic features precede the formation of CSs and WSs. We found that the majority of temperature extremes were associated with changes in the circulation regime above the North Atlantic (usually described through the NAO phase), which in turn are closely associated with stratospheric circulation, namely PV strength. The majority of WSs were related to an increased intensity of PVs and reflected WAFs over the North Atlantic downward. On the other hand, a WAF pathway from Ural blocking to Greenland blocking through a weak stratospheric PV was more often observed before the CS.

Acknowledgements: I thank NASA and NCEP/NCAR for making the reanalysis data available. I also acknowledge the E-OBS dataset from the EU-FP6 project UERRA (http://www.uerra.eu) and the Copernicus Climate Change Service, and the data providers in the ECA&D project. I thank Professor E. Rimkus (Vilnius University, Lithuania) and Dr. Mostafa E. Hamouda (University of Milano-Bicocca, Italy) for their help with this research, and the anonymous reviewers for their very constructive comments that improved this study. Funding: This research was funded by European Social Fund under grant agreement with the Research Council of Lithuania (LMTLT) [grant number 09.3.3-LMT-K-712-02-0141].

Supplementary Information: The supplementary information related to this article is available online at: http://www.borenv.net/BER/archive/pdfs/ber27/ber27-145-160-supplement.pdf

References

Ambaum M.H.P. & Hoskins, B.J. 2002. The NAO Troposphere–Stratosphere Connection. J. Clim. 15(14): 1969–1978.

Baldwin M.P. & Dunkerton T.J. 1999. Propagation of the Arctic Oscillation from the stratosphere to the troposphere. J. Geophys. Res. 104(30): 937–946. https://doi.org/10.1029/1999JD900445.

Baldwin M.P. & Dunkerton T.J. 2001. Stratospheric harbingers of anomalous weather regimes. Science. 294(5542):581–584. doi: 10.1126/science.1063315. PMID: 11641495.

Barnes E.A., Samarasinghe S.M., Ebert-Uphoff I. & Furtado J.C. 2019. Tropospheric and stratospheric causal pathways between the MJO and NAO. J. Geophys. Res. Atmos. 124: 9356–9371. https://doi.org/10.1029/2019JD031024.

Butler A.H., Seidel D.J., Hardiman S.C., Butchart N., Birner T. & Match A. 2015. Defining Sudden Stratospheric Warmings. Bull. Am. Meteorol. Soc. 96(11): 1913–1928.

Cai M. & Ren R.C. 2007. Meridional and downward propagation of atmospheric circulation anomalies. Part I: Northern Hemisphere cold season variability. *J. Atmos. Sci.* **64**: 1880–1901. doi:10.1175/JAS3922.1.

Cassou C. 2008. Intraseasonal interaction between the Madden–Julian Oscillation and the North Atlantic Oscillation. Nature. 455(7212): 523–527.

Cornes R., van der Schrier G., van den Besselaar E.J.M. & Jones P.D. 2018. An Ensemble Version of the E-OBS Temperature and Precipitation Datasets. J. Geophys. Res. Atmos. 123(17). doi:10.1029/2017JD028200.

Davini P., Cagnazzo C., Neale R. & Tribbia, J. 2012. Coupling between Greenland blocking and the North Atlantic Oscillation pattern. Geophys. Res. Lett. 39: L14701.

Domeisen D.I.V., Badin G. & Koszalka I.M. 2018. How Predictable Are the Arctic and North Atlantic Oscillations? Exploring the Variability and Predictability of the Northern Hemisphere. *J. Clim. 31*(3): 997–1014.

Douville H. 2009. Stratospheric polar vortex influence on Northern Hemisphere winter climate variability. Geophys. Res. Lett. 36: L18703. doi:10.1029/2009GL039334.

Gečaitė I. 2021. Climatology of Three-Dimensional Eliassen–Palm Wave Activity Fluxes in the Northern Hemisphere Stratosphere from 1981 to 2020. Climate. 9: 124. https://doi.org/10.3390/cli9080124.

Gelaro R., McCarty W., Suárez M.J., Todling R., Molod A., Takacs L., Randles C., Darmenov A., Bosilovich M.G., Reichle R., Wargan K., Coy L., Cullather R., Draper C., Akella S., Buchard V., Conaty A., da Silva A., Gu W., Kim G.K., Koster R., Lucchesi R., Merkova D., Nielsen J.E., Partyka G., Pawson S., Putman W., Rienecker M., Schubert S.D., Sienkiewicz M., Zhao B. 2017. The Modern-Era Retrospective Analysis for Research and Applications, Version 2 (MERRA-2). J Clim. 30(13):5419–5454. doi: 10.1175/JCLI-D-16-0758.1.

Gerber E.P., Orbe C., Polvani L.M. 2009. Stratospheric influence on the tropospheric circulation revealed by idealized ensemble forecasts. Geophys. Res. Lett. 36: L24801. doi:10.1029/2009GL040913.

Harnik N. 2009. Observed stratospheric downward reflection and its relation to upward pulses of wave activity. J. Geophys. Res.114: D08120. doi:10.1029/2008JD010493.

Jahn M. 2015. Economics of extreme weather events: Terminology and regional impact models. Weather. Clim. Extremes .10B: 29–39. https://doi.org/10.1016/j.wace.2015.08.005.

Jia X., Yang S., Song W., He B. 2014. Prediction of wintertime Northern Hemisphere blocking by the NCEP Climate Forecast System. J. Meteorol. Res. 28: 76–90.

Karpechko A.Y., Hitchcock P., Peters D.H.W., Schneidereit A. 2017. Predictability of downward propagation of major sudden stratospheric warmings. Q. J. R. Meteorol. Soc. 143(704): 1459–1470. https://doi.org/10.1002/qj.3017.

Kautz L.-A., Martius O., Pfahl S., Pinto J.G., Ramos A.M., Sousa P.M., Woollings T. 2022. Atmospheric blocking and weather extremes over the Euro-Atlantic sector – a review. Weather Clim. Dynam. 3: 305–336. https://doi.org/10.5194/wcd-3-305-2022.

Kidston J., Scaife A., Hardiman S. et al. 2015. Stratospheric influence on tropospheric jet streams, storm tracks and surface weather. Nature Geosci 8: 433–440. https://doi.org/10.1038/ngeo2424.

Kidston J., Scaife A.A., Hardiman S.C., Mitchell D.M., Butchart N., Baldwin M. P, Gray L.J. 2015. Stratospheric influence on tropospheric jet streams, storm tracks and surface weather. Nat. Geosci. 8: 433–440. https://doi.org/10.1038/ngeo2424.

Kim S-J, Choi H-S. 2021. Role of polar vortex weakening in cold events in central Asia during late winter. Polar Sci. 30: 100640. https://doi.org/10.1016/j.polar.2021.100640.

Klotzbach P., Abhik S., Hendon H.H. et al. 2019. On the emerging relationship between the stratospheric Quasi-Biennial oscillation and the Madden-Julian oscillation. Sci. Rep. 9: 2981. https://doi.org/10.1038/s41598-019-40034-6.

Kodera K., Mukougawa H. & Fujii A. 2013. Influence of the vertical and zonal propagation of stratospheric planetary waves on tropospheric blockings. J. Geophys. Res. Atmos. 118: 8333–8345. doi:10.1002/jgrd.50650.

Kodera K., Mukougawa H., & Itoh S. 2008. Tropospheric impact of reflected planetary waves from the stratosphere. Geophys. Res. Lett. 35: L16806. doi:10.1029/2008GL034575.

Kodera K., Mukougawa H., Maury P., Ueda M., & Claud C. 2016. Absorbing and reflecting sudden stratospheric warming events and their relationship with tropospheric circulation: Absorbing and reflecting sudden warmings. J. Geophys. Res. Atmos. 121(1): 80–94. https://doi.org/10.1002/2015jd023359.

Kolstad E.W., Breiteig T., & Scaife A.A. 2010. The association between stratospheric weak polar vortex events and cold air outbreaks in the Northern Hemisphere. Quart. J. Roy. Meteor. Soc. 136: 886–893. https://doi.org/10.1002/qj.620.

Kretschmer M., Cohen J., Matthias V. et al. 2018. The different stratospheric influence on cold-extremes in Eurasia

and North America. npj. Clim. Atmos. Sci. 1: 44. https://doi.org/10.1038/s41612-018-0054-4.

Lee R.W., Woolnough S.J., Charlton-Perez A.J. & Vitart F. 2019. ENSO modulation of MJO teleconnections to the North Atlantic and Europe. Geophys. Res. Lett. 46: 13535– 13545. https://doi.org/10.1029/2019GL084683.

Limpasuvan V., Thompson D.W.J. & Hartmann D.L. 2004. The Life Cycle of the Northern Hemisphere Sudden Stratospheric Warmings, *J. Clim. 17*(13): 2584–2596.

Marshall A.G. & Scaife A.A. 2009. Impact of the QBO on surface winter climate. J. Geophys. Res. 114: D18110. doi:10.1029/2009JD011737.

McMichael A.J., Powles J.W., Butler C.D. & Uauy R. 2007. Food, livestock production, energy, climate change, and health. Lancet. 370(9594): 1253–1263. https://doi.org/10.1016/S0140-6736(07)61256-2.

Messori G., Kretschmer M., Lee S.H., Matthias V. 2022. Stratospheric Wave Reflection Events Modulate North American Weather Regimes and Cold Spells. Weather Clim. Dynam. Discuss. [preprint]. https://doi.org/10.5194/wcd-2022-18.

Mitchell D.M., Gray L.J., Anstey J., Baldwin M.P. & Charlton-Perez A J. 2013. The Influence of Stratospheric Vortex Displacements and Splits on Surface Climate. J. Clim. 26(8): 2668–2682.

Nath D., Chen W., Zelin C., Pogoreltsev A.I. & Wei K. 2016. Dynamics of 2013 Sudden Stratospheric Warming event and its impact on cold weather over Eurasia: Role of planetary wave reflection. Sci. Rep. 6:24174. doi: 10.1038/srep24174.

Pang B., Scaife A.A., Lu R. & Ren R. 2021. Asymmetric Impact of the Scandinavian Pattern on Stratospheric Circulation Anomalies, *J. Clim. 34*(23): 9293–9303.

Perlwitz J. & Harnik N. 2003. Observational evidence of a stratospheric influence on the troposphere by planetary wave reflection. J. Clim. 16: 3011–3026. doi:10.1175/1520-0442(2003)016<3011:OEOASI>2.0.CO;2.

Perlwitz J. & Harnik N. 2004. Downward coupling between the stratosphere and troposphere: The relative roles of wave and zonal mean processes. J. Clim. 17: 4902–4909. doi:10.1175/JCLI-3247.1.

Qian W., Yu T. & Du J. 2016. A unified approach to trace surface heat and cold events by using height anomaly. Clim. Dyn. 46: 1647–1664. https://doi.org/10.1007/s00382-015-2666-2.

Quandt L.A., Keller J.H., Martius O. & Jones S.C. 2017. Forecast variability of the blocking system over Russia in summer 2010 and its impact on surface conditions. Wea. Forecasting. 32: 61–82. https://doi.org/10.1175/WAF-D-16-0065.1.

Scaife A.A., Baldwin M.P., Butler A.H., Charlton-Perez A.J., Domeisen D.I.V., Garfinkel C.I., Hardiman S.C., Haynes P., Karpechko A.Y., Lim E.-P., Noguchi S., Perlwitz J., Polvani L., Richter J.H., Scinocca J., Sigmond M., Shepherd T.G., Son S.-W., Thompson D.W.J. 2022. Long-range prediction and the stratosphere. Atmos. Chem. Phys. 22: 2601–2623. https://doi.org/10.5194/acp-22-2601-2022.

Scott R.K. & Polvani L.M. 2004. Stratospheric control of upward wave flux near the tropopause., Geophys. Res. Lett. 31: L02115. doi:10.1029/2003GL017965.

Shaw T.A. & Perlwitz J. 2013. The Life Cycle of Northern Hemisphere Downward Wave Coupling between the Stratosphere and Troposphere. *J. Clim. 26*(5): 1745–1763.

Shi C., Xu T., Guo D. & Pan Z. 2017. Modulating Effects of Planetary Wave 3 on a Stratospheric Sudden Warming Event in 2005. J. Atmos. Sci. 74(5): 1549–1559.

Sigmond M., Scinocca J., Kharin V. et al. 2013. Enhanced seasonal forecast skill following stratospheric sudden warmings. Nature Geosci. 6: 98–102. https://doi.org/10.1038/ngeo1698.

Spaeth J. Birner T. 2022. Stratospheric modulation of Arctic Oscillation extremes as represented by extended-range ensemble forecasts. Weather Clim. Dynam. 3: 883–903. https://doi.org/10.5194/wcd-3-883-2022.

Thompson D.W.J. & Wallace J.M. 1998. The Arctic Oscillation signature in the wintertime GPH and temperature fields. Geophys. Res. Lett. 25: 1297–1300.

Thompson D.W.J., Baldwin M.P. & Wallace J.M. 2002. Stratospheric Connection to Northern Hemisphere Wintertime Weather: Implications for Prediction. J. Clim. 15(12): 1421–1428.

Tomassini L., Gerber E.P., Baldwin M.P., Bunzel F. & Giorgetta M. 2012. The role of stratosphere-troposphere coupling in the occurrence of extreme winter cold spells over northern Europe. J. Adv. Model. Earth Syst. 4: M00A03. doi:10.1029/2012MS000177.

Tomczyk A.M. & Bednorz E. 2019. Heat waves in Central Europe and tropospheric anomalies of temperature and GPHs. Int J Climatol. 39: 4189– 4205. https://doi.org/10.1002/joc.6067.

Tripathi O.P., Baldwin M., Charlton-Perez A., Charron M., Eckermann S.D., Gerber E., Harrison R.G., Jackson D.R., Kim B.M., Kuroda Y., Lang A., Mahmood S., Mizuta R., Roff G., Sigmond M. & Son S.W. 2015. Review: the predictability of the extra-tropical stratosphere on monthly timescales and its impact on the skill of tropospheric forecasts. Q. J. R. Meteorol. Soc. 141(689): 987–1003. doi: https://doi.org/10.1002/qj.2432.

Tyrlis E., Manzini E., Bader J., Ukita J., Nakamura H. & Matei D. 2019. Ural blocking driving extreme Arctic sea ice loss, cold Eurasia, and stratospheric vortex weakening in autumn and early winter 2016–2017. J. Geophys. Res. Atmos. 124: 11313–11329. https://doi.org/10.1029/2019JD031085.

Zhang M., Yang X.-Y., Huang Y. 2022. Impacts of sudden stratospheric warming on extreme cold events in early 2021: An ensemble-based sensitivity analysis. Geophys. Res. Lett. 49: e2021GL096840. https://doi.org/10.1029/2021GL096840.